2019

Flow Reorganization in an Anthropogenically Modified Tidal Channel Network: An Example From The Southwestern Ganges-Brahmaputra-Meghna Delta

R. L. Bain

Rip P. Hale
Old Dominion University, rphale@odu.edu

S. L. Goodbred

Original Publication Citation

Bain, R. L., Hale, R. P., & Goodbred, S. L. (2019). Flow reorganization in an anthropogenically modified tidal channel network: An example from the southwestern Ganges-Brahmaputra-Meghna Delta. *Journal of Geophysical Research: Earth Surface, 124*(8), 2141-2159. doi:10.1029/2018JF004996

JGR Earth Surface

RESEARCH ARTICLE
10.1029/2018JF004996

Flow Reorganization in an Anthropogenically Modified Tidal Channel Network: An Example From the Southwestern Ganges-Brahmaputra-Meghna Delta

R. L. Bain[1], **R. P. Hale**[2], **and S. L. Goodbred**[1]

[1]Department of Earth and Environmental Sciences, Vanderbilt University, Nashville, TN, USA, [2]Department of Ocean, Earth and Atmospheric Sciences, Old Dominion University, Norfolk, VA, USA

Key Points:
- Channel scouring and widening suggest a local increase in discharge exchange between two large, interconnected tidal channels
- This deviation from the nearby trend of widespread channel infilling is a consequence of internal flow reorganization
- Anthropogenic modification of tidal delta plain environments may significantly alter the dynamics of looping channel networks

Supporting Information:
- Supporting Information S1

Correspondence to:
S. L. Goodbred,
steven.goodbred@vanderbilt.edu

Citation:
Bain R. L., Hale, R. P., & Goodbred, S. L. (2019). Flow reorganization in an anthropogenically modified tidal channel network: An example from the southwestern Ganges-Brahmaputra-Meghna Delta. *Journal of Geophysical Research: Earth Surface*, *124*, 2141–2159. https://doi.org/10.1029/2018JF004996

Received 8 JAN 2019
Accepted 10 JUL 2019
Accepted article online 17 JUL 2019
Published online 17 AUG 2019

Abstract We examine variations in discharge exchange between two parallel, 1- to 2-km-wide tidal channels (the Shibsa and the Pussur) in southwestern Bangladesh over spring-neap, and historical timescales. Our objective is to evaluate how large-scale, interconnected tidal channel networks respond to anthropogenic perturbation. The study area spans the boundary between the pristine Sundarbans Reserved Forest, where regular inundation of the intertidal platform maintains the fluvially abandoned delta plain, and the anthropogenically modified region to the north, where earthen embankments sequester large areas of formerly intertidal landscape. Estimates of tidal response to the embankment-driven reduction in basin volume, and hence tidal prism, predict a corresponding decrease in size of the mainstem Shibsa channel, yet the Shibsa is widening and locally scouring even as the interconnected Pussur channel faces rapid shoaling. Rather, the Shibsa has maintained or even increased its pre-polder tidal prism by capturing a large portion of the Pussur's basin via several "transverse" channels that are themselves widening and deepening. We propose that an enhanced tidal setup in the Pussur and the elimination of an effective Shibsa-Pussur flow barrier are driving this basin capture event. These results illustrate previously unrecognized channel interactions and emphasize the importance of flow reorganization in response to perturbations of interconnected, multichannel tidal networks that characterize several large tidal delta plains worldwide.

1. Introduction

Tidal energy influences coastal morphology and nearshore sedimentation worldwide (Davies, 1964), with even small-amplitude tides capable of modifying river- or wave-driven transport and deposition (Dashtgard et al., 2012; Leonardi et al., 2013). In almost all shallow water tidal environments, tidal channels are a prominent feature influencing regional morphodynamic behavior. Specifically, non-linear frictional distortion influences the symmetry and the amplitude of the tidal waveform as it propagates upchannel. The result is an unequal duration of the rising and falling limbs, with the shorter limb necessarily displaying higher flow velocities. This has profound implications for determining the net sediment transport direction and long-term system stability (e.g., Blanton et al., 2002; Dronkers, 1986; Friedrichs & Aubrey, 1988; Mazda et al., 1995; Speer & Aubrey, 1985; Wells, 1995).

Most prior research addressing flow behavior in tidal channels emphasizes two end-member cases. First, much focus has been placed on channel formation and stability in tidal wetland environments. Tidal behavior in these systems is strongly influenced by overbank exchange with the intertidal platform (e.g., Blanton et al., 2002; Pethick, 1980), but their short spatial scale (10^0 to 10^1 km) prevents the development of differential water surface elevations needed to drive channelized flow between adjacent tidal basins. Indeed, these studies are typically able to assume instantaneous tidal propagation across the marsh (e.g., Boon, 1973; Fagherazzi et al., 2008; Pethick, 1980; Seminara et al., 2010). However, this assumption is quickly violated when considering tidal hydrodynamics in systems that span hundreds of kilometers, such as the Ganges-Brahmaputra-Meghna tidal delta plain, where cross-system propagation times may exceed several hours and non-negligible lateral surface gradients may develop between neighboring channels.

A second tidal setting commonly addressed in the literature is the classic "funnel-shaped" estuary. In contrast to small-scale tidal wetlands, an estuarine channel may display tidal oscillations hundreds of kilometers

inland from the coast, like the Ganges-Brahmaputra-Meghna system. However, the typically small ratio of intertidal platform to channelized area in tidal estuaries allows the simplifying assumption that platform flooding has negligible effect on the tidal hydrodynamics (e.g., Todeschini et al., 2008). The number of channels in such networks also tends to be low. Among the best studied tidal estuaries in the world (the Amazon, Columbia, Fly, Ord, Pearl, Saint Lawrence, Western Scheldt, and Yangtze), none has more than four outlets at the coast.

Here we present results from a third type of tidal environment, the tidal delta plain, which shares some attributes of tidal wetlands and estuaries but is nevertheless distinct in its governing physical processes. Like tidal wetland settings, deltas with a large vertical tidal range often display an extensive intertidal platform, making it unreasonable to neglect the effects of overbank flow when analyzing channel behavior. However, it is also unreasonable to characterize tidal delta plain dynamics using the results of marsh inundation studies due to the difference in spatial scale. Delta plains are spatially extensive and able to develop non-negligible water surface gradients along the channel profiles. Additionally, the length of coastline (200–300 km) and the total number of channel outlets (~10–20) typically exceed those of the traditional estuarine environment, creating conditions that favor the development of both along-coast and interchannel gradients in tidal phase and amplitude. Large differences in freshwater discharge from upstream further contribute to these gradients, as many of the channels may receive no direct fluvial input. Emerging from these controls are looping structures (e.g., Tejedor et al., 2015), which allow for channelized flow exchange between the delta plain's dominant channels and define a characteristic topological feature of these channel network systems.

Among of the largest (10 to 20×10^3 km^2) and most prevalent examples of these looping tidal channel networks are the south Asian megadeltas, including the Ganges-Brahmaputra-Meghna Delta (GBMD), Indus (Giosan et al., 2006), and Ayeyarwady (Goodbred & Saito, 2012). Other examples of expansive tidal delta plains (5 to 10×10^3 km^2) with looping networks include the Orinoco in South America (Aslan et al., 2003), the Kikori-Purari in Papua New Guinea (Fagherazzi, 2008), and the Sesayap in eastern Borneo. Each of these systems is characterized by an extensive intertidal platform with highly interconnected channels, yet these systems and their corresponding morphodynamic processes have not been well studied, and many remain largely undescribed. Of these, the GBMD has perhaps received the most attention (e.g., Bricheno et al., 2016; Chatterjee et al., 2013; Hale et al., 2019; Pethick & Orford, 2013; Shaha & Cho, 2016), and we build on this knowledge with the present study.

The relevant literature on this type of system includes several recent publications which characterize tidal hydrodynamics in smaller tidal delta plain environments with interconnected channels, including the ~500 km^2 Berau (Buschman et al., 2010, 2013) and ~1,500 km^2 Mahakam Delta (Sassi et al., 2011, 2013). These results provide a conceptual framework for understanding how mass and energy propagate through looping, interconnected systems. Key findings include the observation that tides influence discharge and sediment transport tens to >100 km inland of the coast, and adjacent tidal channels often display contrasting hydrodynamic behavior. In this paper, we focus on the question of how hydrodynamic variation among interconnected channels influences channel stability within such looping tidal systems.

The question of deltaic channel stability is broadly relevant considering its implications for stratigraphic interpretation, navigation, and sustainable delta management, yet the mechanisms governing tidal channel network reorganization and the rate at which these mechanisms operate are poorly constrained. For example, although deltaic tidal channels tend to be less mobile than their non-tidal counterparts (Hoitink et al., 2017; Lentsch et al., 2018; Rossi et al., 2016), Fagherazzi (2008) found that tidal deltas self-organize such that a perturbation to the network will result in a sudden, widespread reorganization. Given the vulnerability of human populations residing on tidal systems and the tendency for anthropogenic activity to "perturb" deltaic environments (e.g., Ericson et al., 2006; Syvitski & Saito, 2007; Syvitski et al., 2009), it is critical to evaluate the stability of tidal channel networks under present and future human influence. Our objectives for this paper are thus (1) to characterize the ongoing, large-scale reorganization of a tidal channel network in the western GBMD, (2) to propose a physical mechanism driving the channels' response to anthropogenic modification of the natural system, and (3) to discuss the implications of our observations for other less studied tidal delta plain environments.

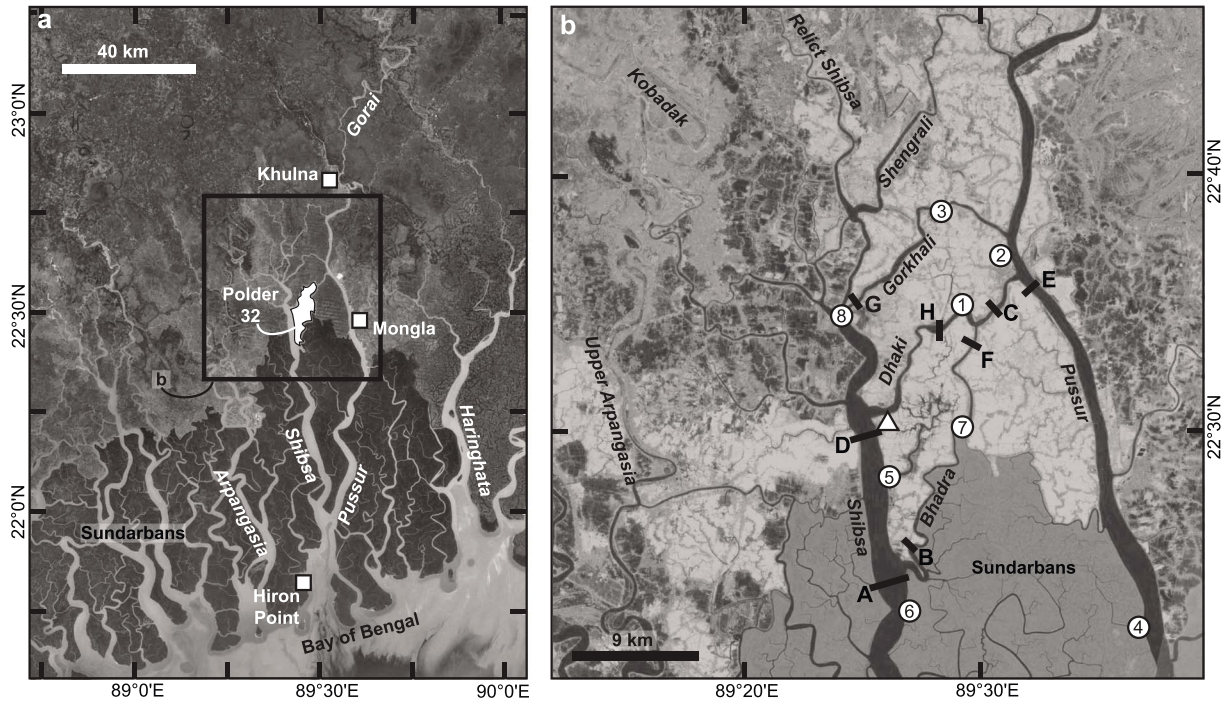

Figure 1. (a) Satellite image of southwest Bangladesh with major channels labeled. The dark region in the southern half of the image is the Sundarbans Reserved Forest, a pristine intertidal mangrove environment; the lighter region to the north is embanked agricultural landscape. Our study focuses on the channels surrounding Polder 32, an embanked island that suffered catastrophic flooding during Cyclone Aila in 2009. The white squares show the location of Hiron Point, Mongla, and Khulna, which were examined in an earlier study by Pethick and Orford (2013). (b) Configuration of the transverse channels connecting the Shibsa and Pussur Rivers in the Polder 32 region. The thick black lines indicate acoustic Doppler current profiler transects from the 2015 monsoon season, with letters corresponding to Table 1. Numbered white circles indicate sites of short-term tide gauging during the same period. The white triangle shows the location of the Gonari meteorological monitoring station. Labels are as follows: A = Shibsa South acoustic Doppler current profiler transect from Hale et al. (2019); B = Bhadra South; C = Dhaki East; D = Shibsa North from Hale et al. (2019); E = Chalna South; F = Bhadra North; G = Gorkhali West; H = Dhaki West; 1 = Brick Factory pressure sensor; 2 = Chalna North; 3 = Gorkhali East; 4 = Jongla Forest Station; 5 = Nalian Forest Station; 6 = Shibsa Forest Station; 7 = Sutarkhali Forest Station; 8 = failed sensor at Shibsa Head ferry ghat. Background: (a) undated Google Earth mosaic from Landsat/Copernicus, ©2018 TerraMetrics; (b) Landsat 8 imagery dated 9 February 2017.

2. Study Area

In this project, we examine flow exchange in a looping subnetwork of the GBMD tidal system (Passalacqua et al., 2013). Our primary focus is the Shibsa and Pussur Rivers, two of the primary north-south conduits for tidal discharge in southwest Bangladesh (Figure 1a). The channels initiate at an estuarine bifurcation ~30 km north of the Bay of Bengal and then extend northward for an additional 60 km before reconnecting via four smaller channels (from south to north, the Bhadra, Dhaki, Gorkhali, and Shengrali Rivers; Figure 1b). Throughout this paper, we refer to these smaller, east-west oriented channels as "transverse" channels to emphasize their role in connecting the subparallel Shibsa and Pussur Rivers. The Pussur then extends more than 150 km north as the Gorai River, a Ganges distributary with a modern monsoon-season discharge of 3,000 m^3/s.

The modern spring tide range is approximately 2 m at the coast but amplifies to > 4 m in the upper tidal basin, where the transverse channels reconnect the main channels. This particular part of the study area lies at the boundary between the Sundarbans Reserved Forest, a pristine intertidal mangrove environment covering 10,000 km^2 across Bangladesh and India, and the densely populated, embanked region to the north. The embanked area is low lying, formerly intertidal landscape (Wilson & Goodbred, 2015) that has been cut off from tidal inundation since the 1960s and 1970s due to widespread construction of earthen embankments to form poldered islands. Confounding issues from these structures include tidal amplification (Pethick & Orford, 2013) and embankment failures (Auerbach et al., 2015), both of which illustrate the critical need to characterize regional landscape dynamics as a basis for sustainable human-landscape interactions. More generally, the extensive tidal channel network in southwestern Bangladesh provides

Table 1
Measured or Estimated Monsoon-Season Tidal Prisms in the Polder 32 Region

Site	Survey dates in 2015	Ebb prism, Ω_{ebb} ($\times 10^7$ m^3)	Flood prism, Ω_{flood} ($\times 10^7$ m^3)	Net prism, $\lvert\Omega_{ebb}\rvert - \lvert\Omega_{flood}\rvert$ ($\times 10^7$ m^3)	Source
			Spring tides		
A. Shibsa South	30, 31 Aug	$+47.0 \pm 1.5$	**-51.3**	-4.3 ± 1.5	Hale et al. (2019)
B. Bhadra South	31 Aug	$+4.59 \pm 0.47$	**-3.37**	$+1.22 \pm 0.47$	This study
C. Dhaki East	1, 2 Sep	**+4.73**	**-3.06**	**+1.67**	This study
D. Shibsa North	2 Sep	**+24.1**	**-28.5**	**-4.4**	Hale et al. (2019)
E. Chalna South[a]	(n/a)	$(+16.6 \pm 0.5) + \lvert\Omega_{flood}^{ChalnaS}\rvert$	$\Omega_{flood}^{ChalnaS}$	$+16.6 \pm 0.5$	Systemwide mass balance
			Neap tides		
E. Chalna South	4 Sep	$+9.55 \pm 0.55$	**-4.43**	$+5.12 \pm 0.55$	This study
F. Bhadra North	4 Sep	**+1.00**	**-0.38**	**+0.62**	This study
G. Gorkhali West	5 Sep	$+4.93 \pm 0.49$	**-1.90**	$+3.03 \pm 0.49$	This study
D. Shibsa North	7 Sep	**+18.3**	-10.7 ± 0.6	$+7.6 \pm 0.6$	Hale et al. (2019)
H. Dhaki West	7 Sep	$+4.02 \pm 0.06$	-2.30 ± 0.94	$+1.72 \pm 1.00$	This study
A. Shibsa South	8 Sep	**+26.4**	-18.2 ± 0.6	$+8.2 \pm 0.6$	Hale et al. (2019)

Note. Letters in the table correspond to the transect labels in Figure 1b. Bold text in this table indicates values that were measured directly by acoustic Doppler current profiler. All other volumes were determined by interpolation and/or mass balance.
[a]Although we lack acoustic Doppler current profiler-based discharge measurements from the Chalna South transect during spring tides, balancing the known values of Ω_{net}^{Shibsa} from Hale et al. (2019) and an upstream Gorai input of about 13.4×10^7 m^3 (i.e., 3,000 m^3/s over 12.42 hr; supporting information Figure S9) requires a *net* prism of $(+16.6 \pm 0.5) \times 10^7$ m^3 at the Chalna South transect. This also constrains the minimum possible value for $\Omega_{ebb}^{ChalnaS}$ (which would occur if $\Omega_{flood}^{ChalnaS} = 0$, i.e., the flow does not reverse). Details of the mass balance calculations are available in the supporting information.

an opportunity to broaden our fundamental knowledge of tidal propagation through spatially extensive, interconnected channels under pristine and engineered conditions.

The issues arising over the past few decades also include major navigational disruptions caused by the siltation and abandonment of channels across the study area (e.g., Rahman, 2017). Wilson et al. (2017) determined that over 600 km of large, navigable waterways (formerly 100–300 m wide) have closed or infilled to <30 m width since the 1960s. Ninety-eight percent of these channel closures were located in the embanked region, whereas only 2% of the infilled channels were within the pristine Sundarbans. The authors attributed this widespread channel abandonment to the polder-driven reduction in tidal prism and consequent decrease in channelized flow velocity. The paper by Hale et al. (2019) further demonstrates the order-of-magnitude agreement between the annual suspended sediment load advected into the system from the Bay of Bengal (Rogers et al., 2013), the former rate of sedimentation on the now-embanked tidal platform (Auerbach et al., 2015), and the volume of sediment required to produce such extensive channel infilling (Wilson et al., 2017).

Although narrowing and abandonment dominate the observed regional changes to the tidal channel network, a comparison of the earliest satellite imagery with the modern channel geometry reveals that some channels have actually widened and straightened over the past half-century (Wilson et al., 2017, with additional examples in Figure 2). Among the best examples of this behavior are several of the transverse channels connecting the Shibsa and Pussur. Ground-based observations and multibeam sonar also show prevalent bank erosion and collapse features along the length of the Dhaki and Bhadra transverse channels, as well as the nearby mainstem Shibsa (Reed, 2015). Such observations are consistent with a local increase in flow volume but deviate from the regional trend of channel infilling observed just upstream (Wilson et al., 2017). However, this change in tidal volume cannot be sourced from outside the Shibsa-Pussur tidal basin. Polder construction has eliminated 10^9 m^3 of intertidal storage volume to the north, east, and west of the study area (Pethick & Orford, 2013), and upstream discharge from the Gorai distributary has halved in the past 50 years due to some combination of Ganges water diversion at the Bangladesh-India border (Anwar & Takewaka, 2014; Mirza, 1998; Winterwerp & Giardino, 2012), land-use change in the Gorai catchment (Bharati & Jayakody, 2011) and/or naturally occurring distributary abandonment as the Ganges migrates eastward

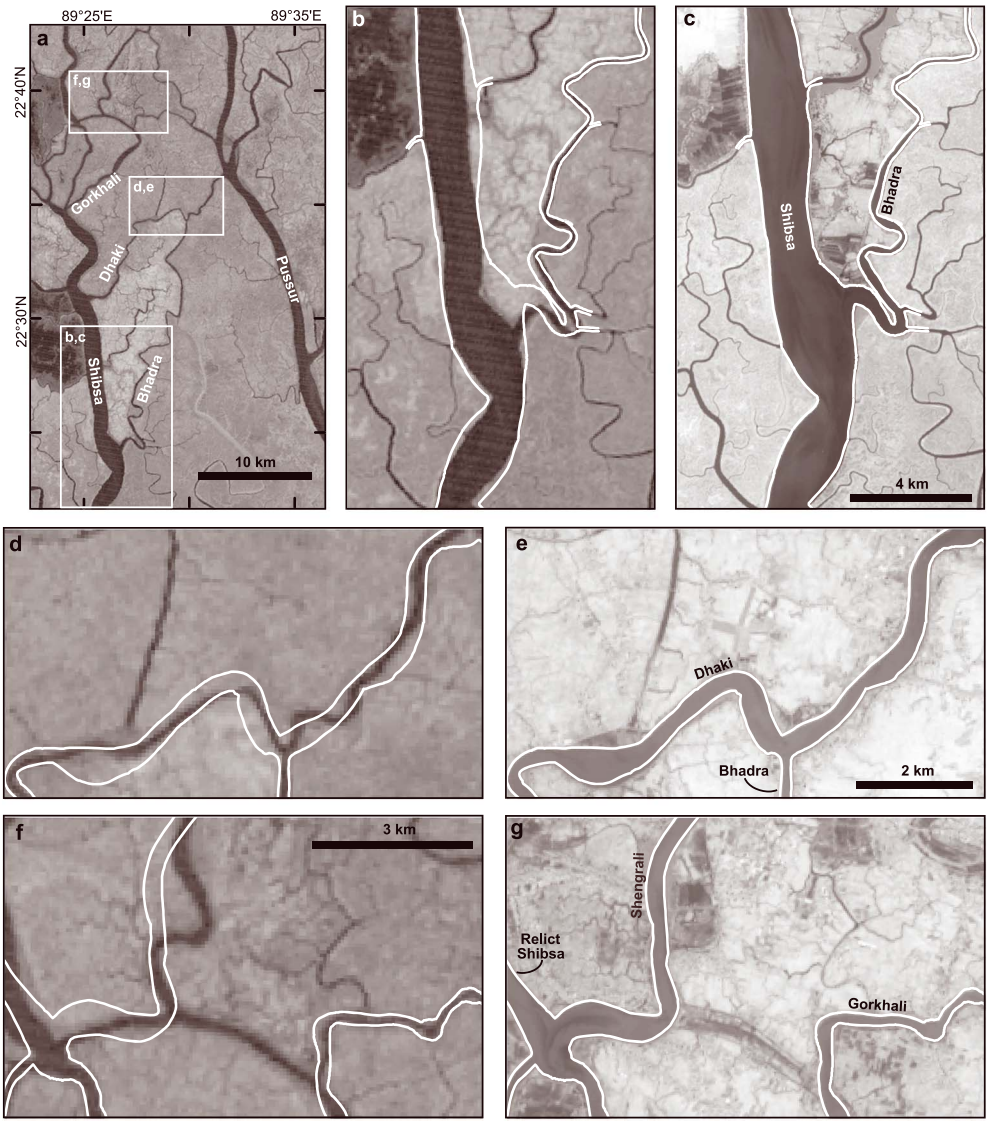

Figure 2. Examples of channel widening and straightening in the Shibsa, Bhadra, Dhaki, Gorkhali, and Shengrali channels. (a) Index map showing the location of frames b–g. (b–g) Paired images comparing the channel geometry on 11 December 1972 (Landsat 1, Band 7–NIR) on the left and 18 February 2017 (Landsat 8, Band 5–NIR) on the right. Both images were acquired around low water during the spring-neap transition. The white lines, which are identical in each pair of images, show the low water line on 11 January 2015. These were manually digitized from high-resolution DigitalGlobe imagery in Google Earth.

(Allison et al., 2003). Any increase in discharge through the transverse channels connecting the Shibsa and Pussur must instead be a consequence of internal flow reorganization. In this paper, we present field data quantifying the volume of water conveyed by the modern transverse channels. We then analyze the modern and pre-polder channel configurations to examine how the magnitude of exchange between the Shibsa and Pussur channels has changed over the past 50 years. Finally, we evaluate these results in the context of other tidal systems and propose a physical mechanism for our observations.

3. Methods

We quantified channel reorganization and decadal-scale discharge variation using a combination of field measurements and GIS-based calculations. Field data were collected over the 2-week period from 27 August to 9 September 2015, encompassing one spring-neap cycle during peak monsoon conditions and maximum Gorai discharge.

3.1. Tidal Elevation Measurements

An assortment of water pressure gauges recorded high-frequency time series of the local tidal oscillations at seven locations in the Polder 32 region of southwest Bangladesh (Figures 1a and 1b). An eighth instrument at Shibsa Head failed after becoming tangled in a fishing net. The sampling interval at each site was determined by available instrument memory but did not exceed $\Delta t = 10$ min. We converted the raw pressure measurements to water depth using a conversion factor of 9.9 kPa/m, which is consistent with the regionally and temporally averaged water temperature of 30.0 °C and conductivity of 32.6 mS/cm. As we were unable to survey the instruments to a common vertical datum, analysis of these data sets is limited to local tidal behavior and cannot provide absolute elevation differences between stations.

Field limitations required us to deploy six of the instruments at sites with up to 2.9 hr of subaerial exposure during spring tide lows; only the CTD-Diver at Sutarkhali Forest Station remained continuously submerged throughout data collection. We reconstructed the missing data with a cubic spline interpolant, which outperformed several tidal constituent-based methods (e.g., Codiga, 2011; Pawlowicz et al., 2002) for reconstructing the known low water elevations at Sutarkhali. The poor performance of the standard tidal analysis algorithms is partly due to the short time series duration, which in many cases was insufficient to separate the M_2 and S_2 constituents and reconstruct a spring-neap pattern. Additionally, we observe a pronounced variation in the amplitude and phase of the shallow water harmonics depending on platform inundation depth; this cannot be reproduced by an algorithm which time averages these parameters. Section S2 in the supporting information contains a detailed description of the cubic spline algorithm.

3.2. Discharge Measurements

We collected discharge data at six transects across the Bhadra, Dhaki, Gorkhali, and Pussur channels using boat-mounted Sontek M9 acoustic Doppler current profilers (ADCPs) with autonomous GPS positioning. Figure 1b displays the location of each ADCP transect as a thick black line. By convention, we define velocities in the downstream or ebb direction (south or southwest) as positive and velocities in the upstream or flood direction as negative. The instrument automatically extrapolated the measured velocity field to the bed and the banks using the power law velocity profile of Chen (1991) and then internally computed discharge as the flux of the velocity field through the area under the transect. To correct for systematic variation in the measured discharge for left-to-right-bank versus right-to-left-bank boat travel, we averaged the raw discharge values for each pair of consecutive, oppositely oriented transects to produce our final data set (see Norris, 2001, but note that we are averaging two, rather than four, transects due to the rapidly changing tidal conditions in our study area). The tidal prisms Ω_{ebb} and Ω_{flood}, defined as the total volume of water passing through a transect between flow reversals, were then calculated by numerically integrating the discharge curve between its zero crossings.

Challenging local working conditions, including hazardous weather and navigational delays, prevented the ADCP surveys from encompassing a full semidiurnal tidal cycle. We estimated the missing discharge values using the extrapolation procedure from Hale et al. (2019), which we summarize as follows. Beginning from the assumption that discharge variation is negligible between consecutive tidal oscillations, we first translated the data forward or backward in time by one semidiurnal period. We then interpolated between the original and translated measurements using a fourth-degree polynomial constrained by a systemwide mass balance of water transport over a tidal cycle. For certain survey sites where this mass balance was underconstrained, we generated a suite of possible interpolating curves, and this paper reports the range of reasonable values. Additional details about this procedure, including the specific assumptions for each transect, are included in section S3 of the supporting information.

3.3. Upstream Basin Volume Estimates: Present Day

We utilized a simplified channel cross-sectional geometry (Figure 3) to determine the spatial extent of the tidal basin associated with each ADCP transect. Starting with high-resolution (1 m/px) Google Earth imagery, we digitized polygons estimating the water surface area at the lowest low water ($A^{\star}_{LL}$), at the moment of overbanking ($A^{\star}_{OB}$), and at highest high water ($A^{\star}_{HH}$) for 2-km-long channel segments extending upstream from the study area. The starred variables denote local measurements for a discrete channel segment. In the poldered region, we assumed that $A^{\star}_{OB} = A^{\star}_{HH}$. For channel segments adjacent to the Sundarbans, we defined $A^{\star}_{OB}$ using the permanent vegetation line along the channel and estimated $A^{\star}_{HH}$ by drawing "interfluves" separating the quasi-dendritic mangrove creek networks.

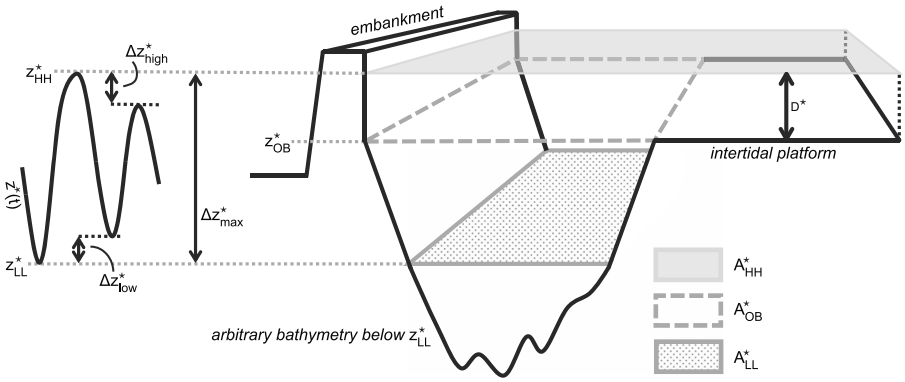

Figure 3. Simplified channel cross sectional geometry used for storage volume calculations. The abbreviations HH and LL refer, respectively, to the elevation of the highest high water and the lowest low water within a given channel segment. The overbank elevation is notated OB. Each channel segment is ~2 km long extending into the page.

For polygons containing one of the deployed pressure gauges, the elevation time series provided local values of the peak tidal range ($\Delta z^\star_{max} = z^\star_{HH} - z^\star_{LL}$, where the subscripts indicate an assumed correspondence to $A^\star_{LL}$ and $A^\star_{HH}$), as well as the offset between the absolute extrema and the high and low water elevations recorded on the date of interest ($\Delta z^\star_{low}$ and $\Delta z^\star_{high}$). We linearly interpolated with along-channel distance to obtain values of $\Delta z^\star_{max}$, $\Delta z^\star_{low}$, and $\Delta z^\star_{high}$ at polygons between two instruments. Upstream of the study area, where we lacked direct measurements of the tidal elevation, we consulted with local fishermen to estimate $\Delta z^\star_{max}$ along the Kobadak, relict Shibsa, and northern Pussur channels (see Table S1 in the supporting information for a detailed summary of these anecdotal tidal ranges).

To estimate the local vertical offset between $z^\star_{OB}$ and $z^\star_{HH}$, we assigned a maximum platform inundation depth $D^\star_{max} = z^\star_{HH} - z^\star_{OB}$ of 0.25 m in the Sundarbans based on in situ observations of the flooding depth. The value of $D^\star_{max}$ then decayed moving northward to a value of 0 at the historical limit of tidal inundation, which we determined by comparing tidal inundation data from Abbas (1966), the upstream extent of soils with a tidal signature (Brammer, 2012), and the boundary between fluvial splay deposits and comparatively featureless topography visible on 1-arcsecond Shuttle Radar Topography Mission (SRTM) data (which approximately corresponds to the base of the upper delta fan system identified by Wilson & Goodbred, 2015). We then assumed a linear change in the value of $A^\star(z)$ between $z^\star_{LL}$ and $z^\star_{OB}$ to calculate the volume of water filling a given channel segment on a specified date.

3.4. Estimates of Pre-polder Tidal Volumes

To estimate the volume of water moving through the system before and immediately following polder construction, we repeated the channel volume calculations described in section 3.3 with several modifications to adjust for unrestricted platform flooding. The local maximum tidal range $\Delta z^\star_{max}$ was reduced based on the amplification trend from Pethick and Orford (2013), with details in section S4 of the supporting information. The overbank area of a given channel segment, $A^\star_{OB}$, was taken as the original embankment position digitized by Wilson et al. (2017), and we assumed that $A^\star_{LL} = 0.8A^\star_{OB}$, which is a representative ratio for the modern polygons. Because platform sedimentation has kept pace with high water amplification (Auerbach et al., 2015), we assumed that the local maximum platform inundation depths $D^\star$ were time invariant over the 50-year study period. Finally, we generated Thiessen polygons from a set of points spaced at 1-km increments along the channel network to produce an estimate of $A^\star_{HH}$ for each channel segment.

In the absence of direct (ADCP based) tidal prism measurements collected prior to polder construction and subsequent channel infilling, we used waveform travel time minimization to estimate whether a given channel segment flooded via the Shibsa or the Pussur. Starting from the channel network GIS shapefile generated by Passalacqua et al. (2013), we updated the channel widths and network connectivity to represent the system's pre-polder geometry. The pre-polder layout was based on a mosaic of the earliest Landsat 1 imagery, dated between 5 November 1972 and 20 February 1973, followed by careful comparison with the *khasland* (i.e., infilled channel) mapping of Wilson et al. (2017) to compensate for possible channel abandonment that may have occurred between polder construction in the 1960s and the satellite acquisition dates. For channel

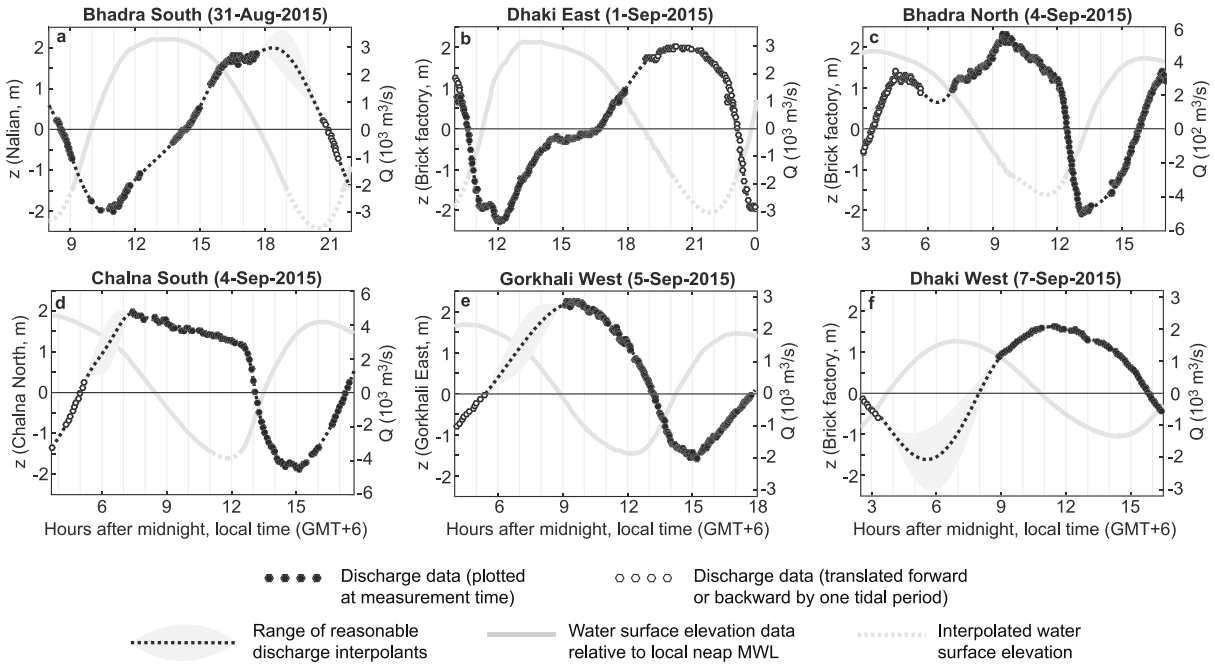

Figure 4. Acoustic Doppler current profiler data and interpolants from six locations in the study area. Black points represent discharge values plotted at the actual time of measurement, whereas white points indicate that the measurement has been translated horizontally by one semidiurnal tidal period. Additional discharge data from this region are available in the paper by Hale et al. (2019). GMT = Greenwich Mean Time; MWL = Mean Water Level.

segments more than 10 km north of the coastline, we assumed that the average depth $\overline{d}^{\star}$ was given by

$$\overline{d}^{\star} = 0.17(w^{\star})^{0.6}, \tag{1}$$

which is the best fit relationship for published non-mouth tidal channel width:depth ratios (compiled from Dury, 1971; Hale et al., 2019; Langbein, 1963; Myrick & Leopold, 1963; Schulz et al., 2015; Wright et al., 1973; Zeff, 1988, 1999, and summarized in supporting information Figure S6). Given the tendency for tidal channels to shoal as they approach open water, equation (1) produced implausibly large depths within the funnel-shaped channel mouths. We corrected for this issue by replacing depths near the coast with soundings from the Defense Mapping Agency (1991).

To produce a first-order estimate of flow paths through the channel network, we assumed that the waveform travel time $T^{\star}$ along each segment scales is

$$T^{\star} \propto \frac{L^{\star}}{\sqrt{g \cdot \overline{d}^{\star}}}, \tag{2}$$

where $L^{\star}$ is the segment length and $g = 9.81$ m/s^2. We then performed a closest facility analysis in ArcMap to determine the fastest route to the Bay of Bengal for 1.2×10^4 points along the channels. This calculation applied Dijkstra's algorithm to calculate the minimum cumulative along-network travel time between the input points and any of a set of 14 points offshore from each of the 14 channel mouths bracketing the Shibsa-Pussur outlet. The 14 target points were located on the 80°M_2 cotidal line to account for the accelerated propagation rate associated with the Swatch of No Ground Canyon in the Bay of Bengal (Sindhu & Unnikrishnan, 2013).

4. Results

In the following sections, we characterize spring-neap variations in net water exchange before addressing how the Shibsa and Pussur tidal basins have changed in size and position since the 1960s. These data reveal complex, tidal range-dependent behavior which has been substantially modified relative to its pre-engineered state.

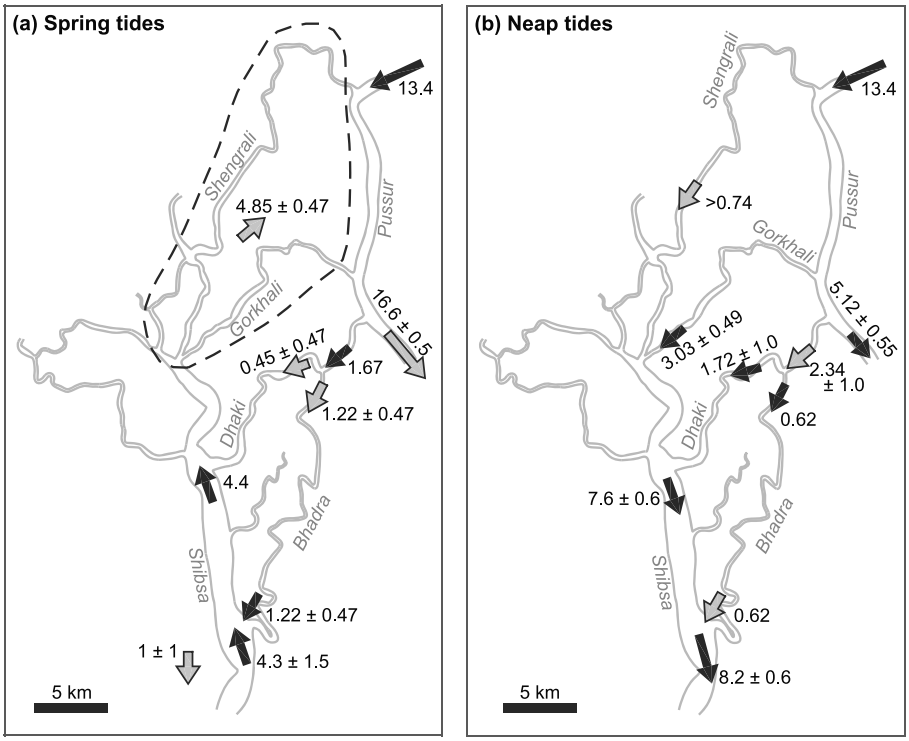

Figure 5. Net monsoon-season tidal prisms in the channels surrounding Polder 32 under (a) spring and (b) neap flow conditions. All numbers have units of 10^7 m^3. Black arrows indicate tidal prisms which were measured by acoustic Doppler current profiler; gray arrows are values required for systemwide mass balance. The dashed line in (a) indicates that the Gorkhali and Shengrali channels together must have a net flood-directed tidal prism of $(-4.85 \pm 0.47) \times 10^7$ m^3; however, we have insufficient data to further constrain how this flow volume is divided among the two channels. For the spring tide mass balance, we have assumed zero net discharge through the Sundarbans east of the Bhadra South acoustic Doppler current profiler transect (Transect B in Figure 1) and a net ebb-directed volume of $(+1 \pm 1) \times 10^7$ m^3 traveling through the Sundarbans near the Shibsa South transect (Transect A). Both assumptions are consistent with the apparent Sundarbans drainage patterns suggested by the small mangrove creeks' quasi-dendritic network geometry.

4.1. Modern Tidal Prisms and Net Circulation Patterns

Here we evaluate our discharge measurements from the transverse channels in the context of Shibsa River discharge data from Hale et al. (2019). The goals of this analysis are (1) to determine the flow division at channel junctions where we were unable to measure discharge directly and (2) to characterize net circulation patterns within the network under spring and neap conditions. Unlike single-inlet systems in which the ebb and flood prisms have equal magnitude, the looping channel network topology in our study area admits the possibility of $|\Omega_{ebb}| \neq |\Omega_{flood}|$. We define the local *net tidal prism* as $\Omega_{net} = \Omega_{ebb} + \Omega_{flood}$, which is positive when $|\Omega_{ebb}| > |\Omega_{flood}|$ and negative for the opposite scenario.

During spring tides, we observe a net ebb-directed flux of water from the Pussur into the Shibsa via both the Dhaki and Bhadra Rivers (Table 1 and Figure 4); however, data from Hale et al. (2019) indicate that the Shibsa South transect conveys a net flood-directed prism of approximately -4.3×10^7 m^3. Because the channel network is effectively a closed system upstream of the study area, one or both of the Gorkhali and Shengrali channels must also be net flood directed, delivering a combined net prism of $(-4.85 \pm 0.47) \times 10^7$ m^3 from the Shibsa into the Pussur (Figure 5a). Moreover, considering the upstream Gorai discharge of approximately 3,000 m^3/s recorded by the Bangladesh Water Development Board at Gorai Railway Bridge during the study period, we estimate a net prism of $(+16.6 \pm 0.5) \times 10^7$ m^3 at Chalna South (Transect E in the Pussur; Figure 1b). The Bangladesh Water Development Board's Gorai discharge data are provided in the supporting information.

Circulation patterns in the study area vary substantially under neap conditions (Figure 5b). For example, the net prism in the Gorkhali is ebb-directed during neap tides, whereas mass balance suggests a flood-directed net prism in this channel under spring-tide flow conditions. Hale et al. (2019) likewise report

Table 2
Storage Volume Between Low and High Water for Various Channel Segments During the Spring Tide on 2 Sep 2015

Polygon description	2 Sep (10^7 m^3)
Shibsa River between Shibsa South and Shibsa North	9.59
Small channel west of Nalian Forest Station and connected Sundarbans[a]	2.55
Bhadra River west of Bhadra South and connected Sundarbans[a]	2.23
Bhadra River east of Bhadra South and connected Sundarbans[a]	2.57
Total storage volume between Shibsa South and Shibsa North	*16.94*
Shibsa River between Shibsa North and Shibsa Head	5.39
Kobadak and Relict Shibsa bifurcates above Shibsa Head	8.07
Dhaki River	3.03
Gorkhali River	2.38
Shengrali River	3.77
Total storage volume above Shibsa North but west of Pussur	*22.64*
Pussur River between Chalna South ADCP transect and Shengrali confluence	5.51
Pussur River from Shengrali confluence to northern Khulna city limits	3.75
Gorai and tributaries from northern Khulna to upstream oscillation limit	6.62
Total storage volume in Pussur/Gorai	*15.88*

Note. The volumes were calculated based on the generalized channel geometry displayed in Figure 3. ADCP = acoustic Doppler current profiler.
[a]Includes storage in main channel, mangrove creeks, and on the intertidal platform during spring tides.

a spring-to-neap reversal in net tidal prism at Shibsa South and Shibsa North. Taking the upper limit of reasonable net neap-tide values measured in the Bhadra, Dhaki, and Gorkhali and the lower bound of the net Shibsa South neap prism indicates that the Shengrali's net neap prism cannot be less than $\Omega_{net}^{Sheng} = +0.74 \times 10^7$ m^3. Due to the uncertainty in the other sites' interpolated discharge values, we are unable to more precisely constrain the value of Ω_{net}^{Sheng}; however, the actual value of the Shengrali's net prism is likely larger than this reported minimum value. In contrast to the positive value of Ω_{net}^{Sheng} during neap tides, the spring tide mass balance suggests that Ω_{net}^{Sheng} is negative. To summarize, comparing the circulation patterns in Figures 5a and 5b indicates that tidal interactions between the Shibsa and the Pussur are strongly dependent on spring versus neap conditions, with the net direction of water transport reversing at several key locations. We will revisit this observation when characterizing the broader significance of our study in section 5.4.

4.2. Spatial Extent of Modern Tidal Basins

To understand how the measured tidal prism is accommodated within the channel network, we route the ADCP-derived tidal prism magnitudes through the available upstream storage volume, which is summarized in Table 2. This exercise provides an estimate of the spatial boundaries of a given transect's tidal basin. Since our ultimate goal is to understand the transverse channels' morphodynamic response to post-polder flow conditions, we here focus on the basin configuration during spring tides when peak flow velocities occur. In this paper, we limit our analysis to the Shibsa North tidal prism (Hale et al., 2019); this eliminates the uncertainty associated with possible net cross-platform exchange through the Sundarbans.

Distributing the flood tidal prism of $|\Omega_{flood}^{ShibN}| = 28.5 \times 10^7$ m^3 measured at Shibsa North on 2 Sep 2015, we find that this volume not only floods the Kobadak and relict Shibsa channels to the west and north but also completely fills the full length of the Dhaki, Gorkhali, and Shengrali channels extending eastward to the Pussur (Figure 6a). Moreover, a residual volume of $\sim 5.9 \times 10^7$ m^3 must flood into the mainstem Pussur channel. As a check on our calculations, we consider whether the remaining storage volume of $\sim 9.7 \times 10^7$ m^3 in the Pussur/Gorai channel upstream of Chalna South could reasonably be filled by non-Shibsa sources. Approximately 6.7×10^7 m^3 of this volume would be filled by the 3,000 m^3/s of Gorai River discharge over a

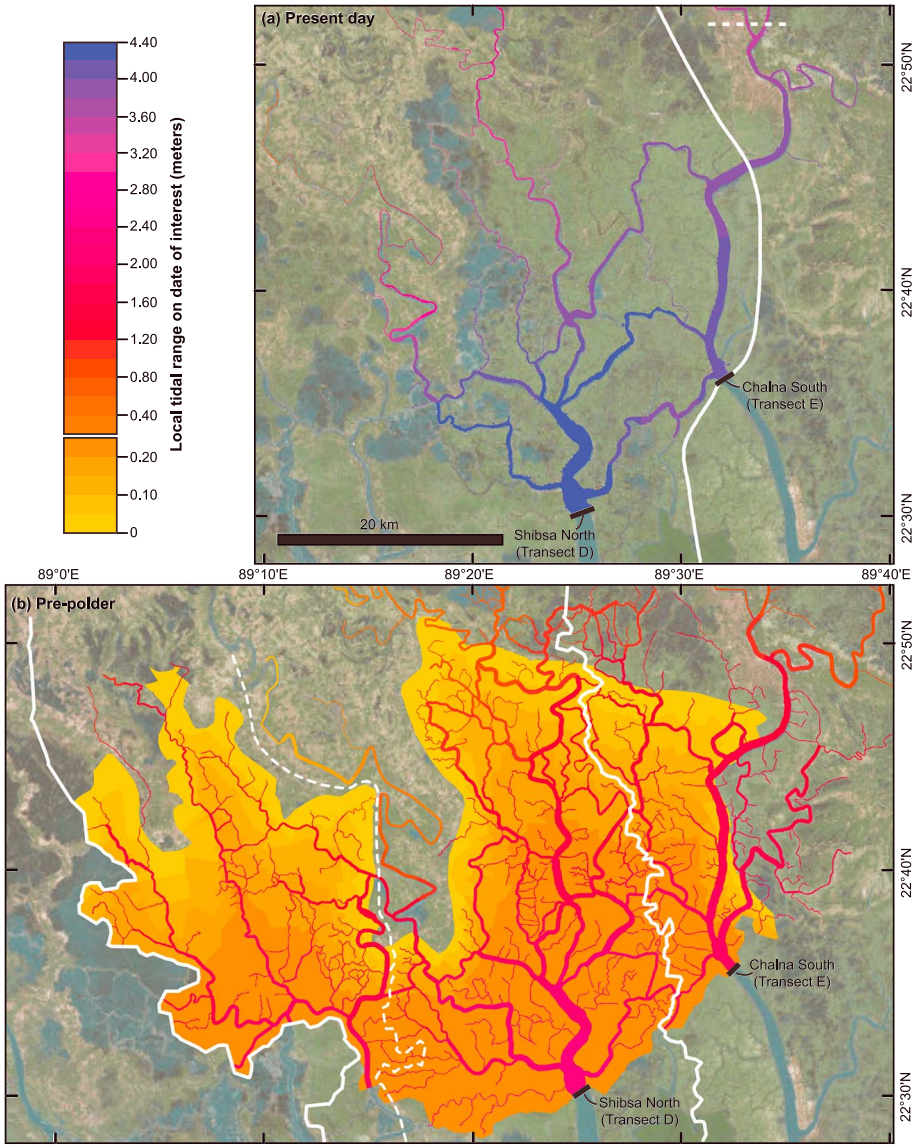

Figure 6. Map of tidal volume above the Chalna South and Shibsa North acoustic Doppler current profiler transects (a) during the midday flooding limb on 2 September 2015 and (b) under peak spring tide conditions for the pre-polder channel configuration. The color scale is the same for both subfigures. The thick white lines indicate estimated tidal basin boundaries. In (a), the Gorai River's discharge over a 6.21-hr flooding limb fills the volume north of the dashed white line; note that this region extends upstream to the limit of vertical oscillation at approximately 23.2°N. For (b), travel time minimization identifies the Shibsa River as the fastest route for tidal waveform travel to the upper Arpangasia basin. However, it is likely that the actual Shibsa-Arpangasia basin boundary was nearer to the dashed line due to discharge mixing from several sources. We include estimates of the Shibsa North basin volume with and without the ambiguous region west of the dashed line; this produces lower and upper bounds for the volume of water conveyed by the Shibsa River. Background: undated TerraColor imagery, ©2018 Earthstar Geographics, obtained through ESRI/ArcMap.

6.21-hr flooding limb (the region north of the dashed line in Figure 6a). The remaining volume in the Pussur would be filled by a spring-tide flood prism at Chalna South of $|\Omega_{\text{flood}}^{\text{ChalnaS}}| = 3 \times 10^7$ m^3, which is comparable in magnitude to the measured flood prism under neap conditions.

4.3. Pre-polder Basin Area and Tidal Volume

One goal of our study is to evaluate how the distribution of water through the modern tidal system differs from its pre-engineered configuration. To accomplish this, we first estimated the pre-polder tidal basin boundaries using waveform travel time minimization, with the results displayed in Figure 6b. The Shibsa

Table 3
Basin Volume North of Polder 32 Before and Immediately After Polder Construction

Location	Pre-polder basin volume ($\times 10^7$ m^3)	Post-polder basin volume ($\times 10^7$ m^3)[a]	Volume lost ($\times 10^7$ m^3)	Percent change
Shibsa Head basin	28.6	13.3	−15.3	−53%
Upper Arpangasia basin[b]	13.0	3.7	−9.3	−72%
Shibsa Head + Arpangasia	**41.6**	**17.0**	**−24.6**	**−59%**
Pussur south of Khulna	12.2	6.6	−5.6	−46%
Pussur north of Khulna	2.9	2.9	0	0%
Pussur total	**15.1**	**9.5**	**−5.6**	**−37%**

[a]Note that the "post-polder" volumes represent the immediate elimination of the tidal platform and small tidal creeks but do not include the additional, gradual loss of volume due to the *khasland* formation described by Wilson et al. (2017). [b]The shortest waveform path calculations indicate that the tide propagating up the Shibsa should be the first to arrive in this basin. However, based on the system geometry observed in 1972 Landsat imagery, it is likely that this region received mixed discharge from the Shibsa and Arpangasia estuaries.

River was the fastest route of tidal waveform arrival for any point between the thick white lines; outside these boundaries, the fastest path was via the Pussur to the east or the Arpangasia to the west. If we make the first-order assumption that discharge also preferentially floods any given location via the fastest travel path, then these lines serve as an estimate of the Shibsa's pre-polder flood basin boundaries. Although we have insufficient discharge data to test the validity of this assumption directly, testing the algorithm on the modern system configuration demonstrates good agreement with the ADCP-derived Shibsa-Pussur basin boundary (see section S5 in the supporting information for details). Moreover, we apply two geometrical arguments to evaluate the validity of our results in the following paragraphs.

First, the travel time minimization algorithm suggests that the Shibsa-Pussur basin boundary was positioned quasi-equidistant from the two channels prior to polder construction (Figure 6b). To test whether the resulting size of the Pussur tidal basin is reasonable, we note that the Gorai's reported monsoon-season discharge of 5,500 m^3/s in 1964 (Winterwerp & Giardino, 2012) would deliver 12.3×10^7 m^3 of water to the Pussur basin above Chalna South over a 6.21-hr rising limb. Under the assumption of negligible net discharge through the transverse channels, which is reasonable given their small pre-polder width, this entire Gorai-contributed volume would necessarily be stored somewhere in the Pussur basin. Meanwhile, the travel time minimization algorithm indicates a Pussur basin volume of 15.1×10^7 m^3 prior to poldering; this corresponds to the region east of the Shibsa basin outline in Figure 6b. The difference of 2.8×10^7 m^3 is the same order of magnitude as the measured Chalna South flood prism (Table 1), suggesting that this volume of water could reasonably enter the basin via a northward directed flow along the Pussur. However, even if the remaining 2.8×10^7 m^3 of water entered this region via the Shibsa (shifting the Shibsa-Pussur basin boundary slightly to the east), the Shibsa still could not have flooded into the Pussur to the extent observed under modern conditions.

Second, we apply published relationships between tidal prism and channel hydraulic geometry to test whether the travel time minimization algorithm generates a reasonable estimate of the channels' respective basin sizes. Empirical fitting (e.g., Jarrett, 1976; O'Brien, 1931, 1969) and numerical models (D'Alpaos et al., 2010) support the existence of a power law relationship between tidal prism and the channel's cross-sectional area at mean water, with Ω raised to a power between 0.85 and 1.10. Although these relationships are complicated by a variety of site-specific parameters (Gao & Collins, 1994), we anticipate that published equations from non-engineered tidal systems should produce a rough estimate of the expected values for the pre-polder GBMD. Applying equation (1) to the Shibsa North transect width in the earliest Landsat imagery, we obtain a cross-sectional area of 1.64×10^4 m^2; this corresponds to a predicted tidal prism between 25.0×10^7 m^3 (using the relationship for non-jettied channels from O'Brien, 1969) and 33.4×10^7 m^3 (based on Jarrett, 1976). Meanwhile, the travel time minimization algorithm predicts a pre-polder Shibsa North basin volume of 41.6×10^7 m^3 (Table 3), which includes the upper reaches of the Arpangasia channel to the west. Because

this is substantially higher than the values predicted by the tidal prism-inlet area relationship, we also consider the possibility that the upper Arpangasia basin (corresponding to the region west of the dashed white line in Figure 6b) was instead flooded by the lower Arpangasia channel. This produces a more conservative estimate of 28.6×10^7 m^3 for the pre-polder Shibsa North basin volume. Thus, we report these lower and upper limits for the Shibsa's pre-polder tidal prism, which respectively correspond to the dashed and solid white lines on the western boundary of the Shibsa tidal basin (Figure 6b).

4.4. Immediate Effect of Polder Construction

As a next step in the analysis, we subtract the storage volume eliminated from each channel's tidal basin using the approximate position of the embankments when they were first constructed (Wilson et al., 2017). These calculations indicate a substantial but geographically varied reduction in basin volume due to poldering (Table 3). The Shibsa basin upstream of the Shibsa North transect lost more than half its storage volume as an immediate consequence of polder construction, reducing from a pre-polder spring tide volume of 28.6×10^7 m^3 to a post-polder volume of 13.3×10^7 m^3 (53% volume loss). These numbers assume that no Shibsa discharge was crossing the dashed white line in Figure 6b; however, if we do include the northern Arpangasia basin, then the volume loss increases to 59%. The Pussur's basin above the Chalna South transect lost about 37% of its volume as a direct consequence of polder construction, decreasing from 15.1×10^7 m^3 to 9.5×10^7 m^3. In summary, these pre-polder tidal volume calculations suggest that polder construction eliminated a larger basin volume in the Shibsa relative to the Pussur, which engendered several morphodynamic responses addressed below.

5. Discussion

The analysis of discharge and tidal range measurements, along with complementary GIS-based estimates of modern and historical basin volumes, produces three key results elucidating the channel network's response to anthropogenic modification. First, we observe that the Shibsa River's flood basin boundary has shifted eastward over the past 70 years, from a pre-polder position approximately halfway between the Shibsa and Pussur channels to the modern configuration in which the Shibsa floods a large portion of Pussur's former basin during peak spring conditions (Figure 6). Specifically, of the $\sim 8.9 \times 10^7$ m^3 of tidal water (i.e., total minus Gorai discharge) required to fill the modern Pussur channel above the Chalna South transect during spring tides, the Shibsa North transect supplies about 5.9×10^7 m^3. In other words, ~20% of the total Shibsa North flood prism of -28.5×10^7 m^3 enters the mainstem Pussur channel during the flooding limb. Second, our calculations indicate that polder construction caused a larger immediate volume reduction in the Shibsa basin compared to the Pussur basin, whether measured by absolute volume loss ($> 13.3 \times 10^7$ m^3 versus 5.6×10^7 m^3) or by percent loss (>53% versus 37%). The first and second results both hold despite uncertainty in the precise location of the Shibsa-Arpangasia and Shibsa-Pussur basin boundaries prior to polder construction.

The third major result is the fundamentally different circulation patterns under modern spring versus neap flow conditions (Figure 5). During spring tides, there is a net flux of tidal volume from the Shibsa into the Pussur. Moreover, the entire volume of freshwater contributed from the Gorai River, along with any additional (unmeasured) flood prism at the Chalna South transect, must ebb out of the system via the Pussur channel. In contrast, there is a net flux of water from the Pussur into the Shibsa during neap tides, with a magnitude equivalent to ~60% of the Gorai input from upstream. We discuss the physical significance and broader implications of these three results in the following sections.

5.1. The Conundrum of Basin Volume Reduction Generating Increased Discharge Exchange

Recent literature highlights the systemwide response to polderization in the GBMD, including tidal range amplification (Pethick & Orford, 2013), accelerated relative elevation loss within the polders (Auerbach et al., 2015), and rapid channel infilling in the upper tidal basins (Wilson et al., 2017). The contemporaneity of polder construction and bank retreat in the transverse channels (Reed, 2015; Wilson et al., 2017) suggests that localized channel widening may be yet another distinct response to these large-scale anthropogenic landscape modifications. Considering the power law relationship between tidal prism and channel cross-sectional area (e.g., D'Alpaos et al., 2010; Gao & Collins, 1994; Jarrett, 1976; O'Brien, 1931) and a second power law relationship between channel width and depth (equation (1)), we posit that the widening of the transverse channels over the past half-century reflects a substantial increase in discharge exchange between the Shibsa and Pussur Rivers via the transverse channels.

Despite these seemingly robust observations, establishing a causative link between polder construction and the enhanced discharge exchange is not intuitive due to strong positive feedbacks between storage volume reduction and channelized flow velocity. For example, to explain why 600 km of major channels were progressively infilled and abandoned after polder construction, Wilson et al. (2017) applied the following mass conservation argument. First, disconnecting these tidal channels from their intertidal platform dramatically reduced the volume of water required to fill the upstream basins. This reduction in basin volume subsequently drove a decrease in mean channelized flow velocities, in addition to eliminating the velocity surge associated with bank overtopping (Pethick, 1980). The resulting decline in sediment transport capacity led to rapid channel siltation, particularly in the blind upstream channels. In summary, this sequence of responses generated a strong positive feedback between tidal prism reduction, a continuing decline in local tidal discharge, and channel infilling and abandonment only 10 km upstream of the Polder 32 region (Figure 1).

Reasoning from this morphodynamic feedback pattern, the tidal prism reduction in the Shibsa and Pussur basins (Table 3) should have decreased flow velocities in both channels and consequently induced sedimentation in the adjoining transverse channels. Instead, we observe the opposite: a significant widening and scouring of the transverse channels, consistent with an increase in discharge. Moreover, considering that the Shibsa basin lost a larger percentage of its volume to poldering, the consequences of polder construction should be more pronounced; that is, we would expect siltation to be enhanced in the mainstem Shibsa channel relative to the mainstem Pussur channel. We instead observe that the main Shibsa channel is widening and scouring near Polder 32 (Figure 2; see also Figure S1 in the supporting information for examples of bathymetry), whereas deep-draft shipping along the Pussur faces major disruption due to rapid shoaling (e.g., Rahman, 2017).

Post-polder tidal range amplification within and upstream of the study area (Pethick & Orford, 2013) could be an alternative mechanism for the observed scouring and widening. For example, amplification of sufficient magnitude could enable the channels to maintain their pre-polder tidal prisms by substituting vertical volume between the embankments for horizontal volume on the intertidal platform. Under this scenario, we would expect amplification-generated scouring to be regionally prominent. However, Pethick and Orford (2013) document tidal amplification along the entire Pussur channel, which is noteworthy for its long-term shoaling and interruption of deep-draft shipping. Consequently, there arises neither evidence nor intuition that tidal range amplification has been a direct cause of the observed bank erosion and channel widening along the Shibsa, Dhaki, Gorkhali, and Shengrali channels.

The possibility remains that the observed expansion of the transverse channels is a consequence of naturally occurring distributary network morphodynamics. For example, changes to the system's boundary conditions (e.g., sea level rise in the Bay of Bengal, changes in sediment input, or migration of fluvial distributaries outside of the tidal region) or natural tidal channel competition could also drive flow reorganization. The results of prior studies allow us to eliminate most of these possibilities. First, Wilson et al. (2017) observed that over the ~50-year period since polder construction, 98% of all channel closures occurred in the embanked region of the study area, with only 2% in the Sundarbans. This suggests that the rate of natural channel network migration and reorganization is low enough to be negligible over the time period of interest. Additionally, Pethick and Orford (2013) documented a tidal range increase of only 5.6 mm/year at the coastal station of Hiron Point (Figure 1a) between 1990 and 2011, in comparison to 16.5 mm/year at Mongla and 28.8 mm/year at Khulna. This indicates that the observed tidal amplification is largely generated by internal modifications to the system rather than by sea level rise in the Bay of Bengal. The mass of sediment imported into the study area has also remained relatively constant over the period of interest (Auerbach et al., 2015; Hale et al., 2019; Rogers et al., 2013). Among the system's boundary conditions, the only significant change is the reduction in the Gorai's monsoon-season freshwater discharge from 5,500 m^3/s in 1964 to 3,000 m^3/s in 2015 (Winterwerp & Giardino, 2012). We evaluate the possible influence of upstream Gorai abandonment in section 5.3.

5.2. Relevance of Distributary Bifurcation Dynamics to Tidal Network Behavior

Having demonstrated that basin volume reduction, tidal amplification, and natural network reorganization are unlikely causes of the observed channel widening and scouring, the remaining possibility is that the direct effects of polder construction documented by Pethick and Orford (2013) and Wilson et al. (2017) have forced a reorganization of tidal discharge partitioning among the channels. To explore this idea, we

first suggest that the transverse channels effectively behave as "distributaries" for the bidirectional flow exchanged between the Shibsa and Pussur, and we thus turn to the rich literature on channel bifurcation dynamics to provide context for our measurements. Flow patterns at our study area's channel junctions are complicated by tidal influence, in contrast to the better studied case of unidirectional distributary behavior; however, universal parameters governing flow division at bifurcations are still relevant for understanding the GBMD system.

Given the economic, engineering, and geological significance of deltaic distributaries, considerable effort has been devoted to identifying the parameters that influence morphological stability at bifurcations. These include the width ratio of the two downstream branches (Bolla Pittaluga et al., 2015; Edmonds & Slingerland, 2008; Kleinhans et al., 2011), a gradient advantage making one bifurcate the preferential flow route (Marra et al., 2014), climate-driven changes in basinwide discharge (Edmonds et al., 2010), and secondary flow structures produced by meanders or bedforms upstream of the bifurcation (Kleinhans et al., 2011; Miori et al., 2012; Sassi et al., 2013). Tidal energy further influences bifurcation behavior by inhibiting sediment deposition in non-dominant distributaries (Kästner et al., 2017), modulating discharge partitioning among the downstream branches (Buschman et al., 2010; Sassi et al., 2011; Zhang et al., 2017), and introducing baroclinically driven circulation between the bifurcates if the system is poorly mixed (Buschman et al., 2013; Kim & Voulgaris, 2005; Shaha & Cho, 2016). However, the relative influence of these parameters varies with local network geometry and other system-specific factors such as bed roughness. In the following section, we apply these authors' findings to develop two hypotheses that may explain cause of internal flow reorganization in our study area.

5.3. Alternative Hypotheses Explaining Post-polder Shibsa Basin Expansion

Our first hypothesis is based on the results of Sassi et al. (2011), who combined field data with a numerical model to quantify river-tide interactions in the bifurcating Mahakam Delta. The authors determined that river discharge in the Mahakam is preferentially allocated to the shorter, deeper bifurcate in the absence of tides, but the introduction of tidal oscillations produces a setup in the dominant branch that reduces its gradient advantage and forces a larger-than-expected fraction of the discharge from upstream into the longer bifurcate. By analogy, we hypothesize that post-polder tidal range amplification (Pethick & Orford, 2013) enhanced the tidal setup in the Pussur and forced a greater percentage of Gorai freshwater discharge into the Shibsa. The consequent increase in discharge scoured the beds of the Dhaki and Gorkhali channels and prevented significant sedimentation in the Shibsa. This generated a disparity in the waveform propagation times along these channels, with the present-day Shibsa and Pussur displaying mean celerity values of 11.2 and 8.1 m/s, respectively, over the distance between Hiron Point and the transverse channels. The faster tidal propagation along the Shibsa thus enables its continued dominance over the Pussur.

However, other results from the Berau and Mahakam deltas suggest that under certain conditions, an increase in tidal energy will *enhance* a bifurcation's discharge inequality in favor of the already-dominant channel (Buschman et al., 2010; Zhang et al., 2017). If these results are more representative of the pre-polder GBMD study area, then the first hypothesis may be invalid. As an alternative, we consider the possibility that changes in the Shibsa-Gorai discharge interaction (rather than the Pussur-Gorai discharge interaction, as in the previous paragraph) were the primary cause of flow reorganization. Table 3 indicates that even before polder construction, the spring tide flood basin above Shibsa North was considerably larger (28.6 to 41.6×10^7 m^3) than the basin above the Chalna South transect (15.1×10^7 m^3). If we make the simplifying assumption of no net discharge through the transverse channels, then the maximum tidal prism at Shibsa North was identical to its basin volume, while the maximum ebb prism at Chalna South transect was $\sim 27.4 \times 10^7$ m^3 (i.e., the 15.1×10^7 m^3 filling the basin during the flooding limb plus an additional 12.3×10^7 m^3 of Gorai discharge entering the system from upstream during the 6.21-hr ebbing limb). This disparity in pre-polder basin size is reflected in our estimated values of mean pre-polder celerity between Hiron Point and the transverse channels: 12.0 m/s in the Shibsa versus 11.8 m/s in the Pussur. Our second hypothesis considers that despite the Shibsa's favorable pre-polder celerity, an opposing influx of Gorai discharge into the transverse channels formerly prevented Shibsa's tidal discharge from intruding into the Pussur. The subsequent decline in Gorai discharge eliminated this discharge-related "barrier" between the Shibsa and the Pussur, allowing the Shibsa basin to expand eastward into the Pussur channel despite its greater loss of tidal volume due to polder construction. Analogous behavior has been reported in the Yangtze Delta (Zhang et al., 2017), where the wet season river discharge prevents the tidal intrusion that occurs under lower flow conditions.

The paucity of long-term discharge and tidal range records from the study area prevents us from testing these hypotheses directly. The opposing results of Sassi et al. (2011) versus Buschman et al. (2010) and Zhang et al. (2017) illustrate that the tidal effect at a bifurcation is strongly dependent on system-specific flow parameters. Moreover, the two proposed hypotheses are not mutually exclusive. Given the complexity of the GBMD tidal channel network (Passalacqua et al., 2013), it is plausible that the combined effects of polder construction (leading to an enhanced tidal setup in the Pussur during the monsoon season) and declining freshwater discharge from the Gorai (eliminating the barrier between the Shibsa and the Pussur during the dry season) operated simultaneously to expand the transverse channels.

5.4. The Broader Significance of Tidal Basin Capture

The literature presents numerous examples of channel avulsion events in which bed aggradation or mouth progradation drives channel relocation to a more hydraulically favorable position (see the review by Kleinhans et al., 2013, and references therein), including instances of tidal channel avulsions (Hood, 2010; Pierik et al., 2018). Although our observation of transverse channel flow expansion and Pussur abandonment has avulsion-like characteristics, we avoid reference to a Gorai River "avulsion" from the Pussur into the Shibsa based on the results in Figure 5. These data indicate that although approximately 60% of the Gorai discharge ebbs through the Shibsa River during monsoon-season neap tides, the entire Gorai-contributed volume must ebb via the Pussur during monsoon-season spring tides. The Pussur is thus still the dominant conduit for conveying Gorai discharge to the Bay of Bengal under peak flow conditions. This is further supported by observations of an ~40-cm tidal setup of the Pussur above the Shibsa during the 2014 monsoon season (Shaha & Cho, 2016), which indicates that the Gorai still most strongly influences Pussur's behavior.

Instead, we find that our results are conceptually similar to the tidal flat channel competition model of Toffolon and Todeschini (2006). These authors found that nearby channels in a small-scale tidal flat setting may exist stably if the system is unperturbed. However, introducing a small perturbation to the initially stable system will introduce a positive feedback in which one channel continues to deepen and capture the other channels' intertidal basins. There are several notable differences between these results and our data, including the substantial variation in spatial scale. Moreover, Toffolon and Todeschini (2006) examined isolated channels expanding their basins across the intertidal platform, whereas the channels in our study area are interconnected, and the captured basin volume is positioned inside the channels between the low and high water elevations. However, the broad idea of perturbation-induced tidal basin capture appears relevant to both small-scale tidal wetland and large-scale tidal delta plain settings, although further study is required to examine the specific parameters that govern this behavior in other large-scale systems.

Regardless of the driving mechanism, the results presented herein highlight the unpredictable response of a large-scale tidal channel network to anthropogenic landscape modification. Whereas an isolated tidal channel should shoal in response to a reduction in basin volume (e.g., D'Alpaos et al., 2010; Gao & Collins, 1994; Jarrett, 1976; O'Brien, 1931), we observed certain channels widening and deepening in our study area. This is a consequence of the inherent complexity of distributary bifurcation dynamics, non-linear river-tide interactions, and variable tidal phasing among the network branches. In addition to its theoretical significance, this behavior has practical implications for human welfare, one of which was already realized when widening along the Dhaki and Shibsa channels eroded the embankments protecting Polder 32 (Figure 1a). It was along these margins that five embankment breaches occurred during Cyclone Aila in 2009 (Auerbach et al., 2015). Given that many of the polders in southwest Bangladesh lie well below mean high water, local bank erosion in response to network reorganization substantially enhances the region's flooding risk.

6. Conclusion

Large-scale embankment construction in the southwestern GBMD during the 1960s and 1970s has driven a regional decline in tidal prism and discharge. However, our observations of local bank retreat and scouring suggest a counterintuitive increase in discharge through several east-west oriented, distributary-type channels connecting the Shibsa and the Pussur Rivers. GIS-based analysis of the earliest Landsat imagery indicates that embankment construction had the immediate effect of eliminating between 53% and 59% of the tidal basin volume above Shibsa North versus 37% of the tidal basin volume above Chalna South in the Pussur. Because a tidal channel's hydraulic geometry is closely related to its basin volume, it is reasonable to predict shoaling in both channels, with this effect being somewhat greater in the Shibsa due to its greater initial basin volume loss. Prior studies document rapid sedimentation and abandonment in both the

mainstem Pussur and in numerous tidal creeks in the former Shibsa basin (Wilson et al., 2017). However, the mainstem Shibsa has maintained its pre-polder basin volume by expanding its basin eastward into the pre-polder Pussur basin.

We interpret our data as a local "basin-capture" event driven by polder-induced tidal amplification and changes to the interactions between tidal currents and Gorai River discharge. These results have serious implications for regional flood vulnerability, especially considering that channels experiencing a local discharge increase have an enhanced risk of embankment failure. Of course, non-anthropogenic forcings including sea level rise, variations in sediment supply, channel mouth progradation, and lateral channel migration can also drive changes in channel network morphology. However, the spatial distribution of observed channel abandonment (98% of all channel closures occur in the embanked region, with only 2% in the pristine Sundarbans mangrove forest; Wilson et al., 2017) increases our confidence that Shibsa's expansion into the Pussur basin and the associated widening of the transverse channels is dominantly a product of anthropogenic landscape modifications.

More broadly, our study suggests that interconnected tidal networks worldwide may respond unpredictably to perturbations because flow patterns are able to reorganize as the channels respond to changing boundary conditions. The western GBMD is morphodynamically analogous to several other minimally studied, large-scale tidal delta plain environments, including the Ayeyarwady, Indus, Kikori-Purari, Mahakam, Orinoco, and Sesayap. Due to loops in these systems' channel networks, results from better studied single-channel estuaries have limited relevance for these systems. Recognizing the complex interacting processes that construct and maintain these systems will be invaluable for interpreting responses to previous or ongoing landscape change. Moreover, future tidal delta plain management strategies necessitated by high rates of effective sea level rise should anticipate the possibility of rapid channel reorganization.

Acknowledgments
This research was funded by the Office of Naval Research (award N00014-11-1-0683) and the National Science Foundation (award 1600258–Coastal SEES). We are grateful to Carol Wilson and Paola Passalacqua for providing GIS data, to Jim Best for supplying the ADCPs, to Elizabeth Chamberlain for advice on the manuscript, and to Md. Zahangir "Titas" Alam, Mamun Hasan, Abrar Hossain, Md. Saddam Hossain, Masud Iqbal, Basudeb Kumar, Chelsea Peters, Mike Reed, Chris Tasich, and the crews of the *Bawali*, *Mawali*, and *Kokilmoni* for assisting with data collection and/or analysis. Luca Solari, Andrea D'Alpaos, and two anonymous reviewers provided feedback that greatly improved the original manuscript. The discharge, water level, and spatial data sets generated during this project are available online (doi:10.6084/m9.figshare.7495904.v1).

References

Abbas, B. M. (1966). Control of floods in East Pakistan. In *Scientific Problems of the Humid Tropical Zone Deltas and their Implications: Proceedings of the Dacca Symposium, February 24 to March 2, 1964* (pp. 135–139). Paris: UNESCO.

Allison, M. A., Khan, S. R., Goodbred, S. L., & Kuehl, S. A. (2003). Stratigraphic evolution of the late Holocene Ganges-Brahmaputra lower delta plain. *Sedimentary Geology*, *155*, 317–342. https://doi.org/10.1016/S0037-0738(02)00185-9

Anwar, M. S., & Takewaka, S. (2014). Analyses on phenological and morphological variations of mangrove forests along the southwest coast of Bangladesh. *Journal of Coastal Conservation*, *18*, 339–357. https://doi.org/10.1007/s11852-014-0321-4

Aslan, A., White, W. A., Warne, A. G., & Guevara, E. H. (2003). Holocene evolution of the western Orinoco Delta, Venezuela. *GSA Bulletin*, *115*, 479–498. https://doi.org/10.1130/0016-7606(2003)115

Auerbach, L. W., Goodbred, S. L. Jr., Mondal, D. R., Wilson, C. A., Ahmed, K. R., Steckler, M. S., et al. (2015). Flood risk of natural and embanked landscapes on the Ganges-Brahmaputra tidal delta plain. *Nature Climate Change*, *5*, 153–157. https://doi.org/10.1038/nclimate2472

Bharati, L., & Jayakody, P. (2011). Hydrological impacts of inflow and land-use changes in the Gorai River catchment, Bangladesh. *Water International*, *36*, 357–369. https://doi.org/10.1080/02508060.2011.586200

Blanton, J. O., Lin, G., & Elston, S. A. (2002). Tidal current asymmetry in shallow estuaries and tidal creeks. *Continental Shelf Research*, *22*, 1731–1743. https://doi.org/10.1016/S0278-4343(02)00035-3

Bolla Pittaluga, M., Coco, G., & Kleinhans, M. G. (2015). A unified framework for stability of channel bifurcations in gravel and sand fluvial systems. *Geophysical Research Letters*, *42*, 7521–7536. https://doi.org/10.1002/2015GL065175

Boon, J. D. (1973). Tidal discharge asymmetry in a salt marsh drainage system. *Limnology and Oceanography*, *20*, 71–80. https://doi.org/10.4319/lo.1975.20.1.0071

Brammer, H. (2012). *The physical geography of Bangladesh*. Dhaka: University Press Ltd.

Bricheno, L. M., Wolf, J., & Islam, S. (2016). Tidal intrusion within a mega delta: An unstructured grid modelling approach. *Estuarine, Coastal, and Shelf Science*, *182*, 12–26. https://doi.org/10.1016/j.ecss.2016.09.014

Buschman, F. A., Hoitink, A. J. F., van der Vegt, M., & Hoekstra, P. (2010). Subtidal flow division at a shallow tidal junction. *Water Resources Research*, *46*, W12515. https://doi.org/10.1029/2010WR009266

Buschman, F. A., van der Vegt, M., Hoitink, A. J. F., & Hoekstra, P. (2013). Water and suspended sediment division at a stratified tidal junction. *Journal of Geophysical Research: Oceans*, *118*, 1459–1472. https://doi.org/10.1002/jgrc.20124

Chatterjee, M., Shankar, D., Sen, G. K., Sanyal, P., Sundar, D., Michael, G. S., et al. (2013). Tidal variations in the Sundarbans estuarine system, India. *Journal of Earth System Science*, *122*, 899–933. https://doi.org/10.1007/s12040-013-0314-y

Chen, C. L. (1991). Unified theory on power laws for flow resistance. *Journal of Hydraulic Engineering*, *117*(3), 371–389. https://doi.org/10.1061/(ASCE)0733-9424(1991)

Codiga, D. L. (2011). Unified tidal analysis and prediction using the UTide Matlab functions (Tech. Rep. 2011-01). Narragansett, RI: Graduate School of Oceanography, University of Rhode Island.

D'Alpaos, A., Lanzoni, S., Marani, M., & Rinaldo, A. (2010). On the tidal prism-channel area relations. *Journal of Geophysical Research*, *115*, F01003. https://doi.org/10.1029/2008JF001243

Dashtgard, S. E., MacEachern, J. A., Frey, S. E., & Gingras, M. K. (2012). Tidal effects on the shoreface: Towards a conceptual framework. *Sedimentary Geology*, *279*, 42–61. https://doi.org/10.1016/j.sedgeo.2010.09.006

Davies, J. L. (1964). A morphogenic approach to world shorelines. *Zeitschrift fuer Geomorphologie*, *8*, 127–142.

Defense Mapping Agency (1991). *Bay of Bengal, Bangladesh and India, Raimangal River to elephant point [Map no. 63330, scale 1:300,000]* (9th ed.). Washington, DC: U.S. Defense Mapping Agency Hydrographic/Topographic Center.

Dronkers, J. (1986). Tidal asymmetry and estuarine morphology. *Netherlands Journal of Sea Research*, *20*, 117–131. https://doi.org/10.1016/0077-7579(86)90036-0

Dury, G. H. (1971). Channel characteristics in a meandering tidal channel: Crooked River, Florida. *Geografiska Annaler*, *53*, 188–197. https://doi.org/10.2307/520788

Edmonds, D. A., & Slingerland, R. L. (2008). Stability of delta distributary networks and their bifurcations. *Water Resources Research*, *44*, W09426. https://doi.org/10.1029/2008WR006992

Edmonds, D. A., Slingerland, R., Best, J., Parsons, D., & Smith, N. (2010). Response of river-dominated delta channel networks to permanent changes in river discharge. *Geophysical Research Letters*, *37*, L12404. https://doi.org/10.1029/2010GL043269

Ericson, J. P., Vörösmarty, C. J., Dingman, S. L., Ward, G., & Meybeck, M. (2006). Effective sea-level rise and deltas: Causes of change and human dimension implications. *Global and Planetary Change*, *50*, 63–82. https://doi.org/10.1016/j.gloplacha.2005.07.004

Fagherazzi, S. (2008). Self-organization of tidal deltas. *Proceedings of the National Academy of Sciences*, *105*, 18,692–18,695. https://doi.org/10.1073/pnas.0806668105

Fagherazzi, S., Hannion, M., & D'Odorico, P. (2008). Geomorphic structure of tidal hydrodynamics in salt marsh creeks. *Water Resources Research*, *44*, W02419. https://doi.org/10.1029/2007WR006289

Friedrichs, C. T., & Aubrey, D. G. (1988). Non-linear tidal distortion in shallow well-mixed estuaries: A synthesis. *Estuarine, Coastal and Shelf Science*, *27*, 521–545. https://doi.org/10.1016/0272-7714(88)90082-0

Gao, S., & Collins, M. (1994). Tidal inlet equilibrium in relation to cross-sectional area and sediment transport patterns. *Estuarine, Coastal and Shelf Science*, *38*, 157–172. https://doi.org/10.1006/ecss.1994.1010

Giosan, L., Constantinescu, S., Clift, P. D., Tabrez, A. R., Danish, M., & Inam, A. (2006). Recent morphodynamics of the Indus delta shore and shelf. *Continental Shelf Research*, *26*, 1668–1684. https://doi.org/10.1016/J.CSR.2006.05.009

Goodbred, S. L., & Saito, Y. (2012). Tide-dominated deltas. In R. Davis Jr., & R. Dalrymple (Eds.), *Principles of tidal sedimentology* (pp. 129–150). New York: Springer.

Hale, R., Bain, R., Goodbred, S. L., & Best, J. (2019). Observations and scaling of tidal mass transport across the lower Ganges-Brahmaputra delta plain: Implications for delta management and sustainability. *Earth Surface Dynamics*, *7*, 231–245. https://doi.org/10.5194/esurf-2018-66

Hoitink, A. J. F., Wang, Z. B., Vermeulen, B., Huismans, Y., & Kästner, K. (2017). Tidal controls on river delta morphology. *Nature Geoscience*, *10*, 637–645. https://doi.org/10.1038/ngeo3000

Hood, W. G. (2010). Delta distributary dynamics in the Skagit River Delta (Washington, USA): Extending, testing, and applying avulsion theory in a tidal system. *Geomorphology*, *123*, 154–165. https://doi.org/10.1016/j.geomorph.2010.07.007

Jarrett, J. T. (1976). Tidal prism-inlet area relationships (GITI Report 3) (Tech. rep.) Fort Belvoir, VA: Army Corps of Engineers.

Kästner, K., Hoitink, A. J. F., Vermeulen, B., Geertsema, T. J., & Ningsih, N. S. (2017). Distributary channels in the fluvial to tidal transition zone. *Journal of Geophysical Research: Earth Surface*, *122*, 696–710. https://doi.org/10.1002/2016JF004075

Kim, Y. H., & Voulgaris, G. (2005). Effect of channel bifurcation on residual estuarine circulation: Winyah Bay, South Carolina. *Estuarine, Coastal and Shelf Science*, *65*, 671–686. https://doi.org/10.1016/j.ecss.2005.07.004

Kleinhans, M. G., Cohen, K. M., Hoekstra, J., & Ijmker, J. M. (2011). Evolution of a bifurcation in a meandering river with adjustable channel widths, Rhine delta apex, The Netherlands. *Earth Surface Processes and Landforms*, *36*, 2011–2027. https://doi.org/10.1002/esp.2222

Kleinhans, M. G., Ferguson, R. I., Lane, S. N., & Hardy, R. J. (2013). Splitting rivers at their seams: Bifurcations and avulsions. *Earth Surface Processes and Landforms*, *38*, 47–61. https://doi.org/10.1002.esp.3268

Langbein, W. B. (1963). The hydraulic geometry of a shallow estuary. *International Association of Scientific Hydrology Bulletin*, *8*, 84–94. https://doi.org/10.1080/02626666309493340

Lentsch, N., Finotello, A., & Paola, C. (2018). Reduction of deltaic channel mobility by tidal action under rising relative sea level. *Geology*, *46*, 599–602. https://doi.org/10.1130/G45087.1

Leonardi, N., Canestrelli, A., Sun, T., & Fagherazzi, S. (2013). Effect of tides on mouth bar morphology and hydrodynamics. *Journal of Geophysical Research: Oceans*, *118*, 4169–4183. https://doi.org/10.1002/jgrc.20302

Marra, W. A., Parsons, D. R., Kleinhans, M. G., Keevil, G. M., & Thomas, R. E. (2014). Near-bed and surface flow division patterns in experimental river bifurcations. *Water Resources Research*, *50*, 1506–1530. https://doi.org/10.1002/2013WR014215

Mazda, Y., Kanazawa, N., & Wolanski, E. (1995). Tidal asymmetry in mangrove creeks. *Hydrobiologia*, *295*, 51–58. https://doi.org/10.007/BF00029110

Miori, S., Hardy, R. J., & Lane, S. N. (2012). Topographic forcing of flow partition and flow structures at river bifurcations. *Earth Surface Processes and Landforms*, *37*, 666–679. https://doi.org/10.1002/esp.3204

Mirza, M. M. Q. (1998). Diversion of the Ganges water at Farakka and its effects on salinity in Bangladesh. *Environmental Management*, *22*, 711–722. https://doi.org/10.1007/s002679900141

Myrick, R. M., & Leopold, L. B. (1963). Hydraulic geometry of a small tidal estuary (*Tech. Rep. 422-B*). Washington, DC: United States Government Printing Office.

Norris, J. M. (2001). Policy and technical guidance on discharge measurements using acoustic Doppler current profilers (*Tech. Rep. 2002.02*). Reston, VA: USGS Office of Surface Water.

O'Brien, M. P. (1931). Estuary tidal prisms related to entrance areas. *Civil Engineering*, *1*, 738–739. https://doi.org/10.1002/jgrf.20128

O'Brien, M. P. (1969). Equilibrium flow areas of inlets in sandy coasts. *Journal of Waterways and Harbors Division, Proceedings of the American Society of Civil Engineers*, *95*, 43–52.

Passalacqua, P., Lanzoni, S., Paola, C., & Rinaldo, A. (2013). Geomorphic signatures of deltaic processes and vegetation: The Ganges-Brahmaputra-Jamuna case study. *Journal of Geophysical Research: Earth Surface*, *118*, 1838–1849. https://doi.org/10.1002/jgrf.20128

Pawlowicz, R., Beardsley, B., & Lentz, S. (2002). Classical tidal harmonic analysis including error estimates in MATLAB using T_TIDE. *Computers and Geosciences*, *28*, 929–937. https://doi.org/10.1016/S0098-3004(02)00013-4

Pethick, J. (1980). Velocity surges and asymmetry in tidal channels. *Estuarine and Coastal Marine Science*, *11*, 331–345. https://doi.org/10.1016/S0302-3524(80)80087-9

Pethick, J., & Orford, J. D. (2013). Rapid rise in effective sea-level in southwest Bangladesh: Its causes and contemporary rates. *Global Planetary Change*, *111*, 237–245. https://doi.org/10.1016/j.gloplacha.2013.09.019

Pierik, H. J., Stouthamer, E., Schuring, T., & Cohen, K. M. (2018). Human-caused avulsion in the Rhine-Meuse delta before historic embankment (The Netherlands). *Geology*, *46*, 935–938. https://doi.org/10.1130/G45188.1

Rahman, M. (2017). Study on morphological change and navigation problems of Pussur River in Bangladesh (Master's thesis), Khulna University of Engineering and Technology.

Reed, M. J. (2015). Polder 32: Riverbank morphology in southwestern Bangladesh (Master's thesis), University of Illinois at Champaign-Urbana.
Rogers, K. G., Goodbred, S. L. Jr., & Mondal, D. R. (2013). Monsoon sedimentation on the 'abandoned' tide-influenced Ganges-Brahmaputra delta plain. *Estuarine, Coastal and Shelf Science*, *131*, 297–309. https://doi.org/10.1016/j.ecss.2013.07.014
Rossi, V. M., Kim, W., López, J. L., Edmonds, D., Geleynse, N., Olariu, C., et al. (2016). Impact of tidal currents on delta-channel deepening, stratigraphic architecture, and sediment bypass beyond the shoreline. *Geology*, *44*, 927–930. https://doi.org/10.1130/G38334.1
Sassi, M. G., Hoitink, A. J. F., de Brye, B., Vermeulen, B., & Deleersnijder, E. (2011). Tidal impact on the division of river discharge over distributary channels in the Mahakam Delta. *Ocean Dynamics*, *61*, 2211–2228. https://doi.org/10.1007/s10236-011-0473-9
Sassi, M. G., Hoitink, A. J. F., Vermeulen, B., & Hidayat, H. (2013). Sediment discharge division at two tidally influenced river bifurcations. *Water Resources Research*, *49*, 2119–2134. https://doi.org/10.1002/wrcr.20216
Schulz, E., Schuttelaars, H. M., Gräwe, U., & Burchard, H. (2015). Impact of the depth-to-width ratio of periodically stratified tidal channels on the estuarine circulation. *Journal of Physical Oceanography*, *45*, 2048–2069. https://doi.org/10.1175/JPO-D-14-0084.1
Seminara, G., Lanzoni, S., Tambroni, N., & Toffolon, M. (2010). How long are tidal channels? *Journal of Fluid Mechanics*, *643*, 479–494. https://doi.org/10.1017/S0022112009992308
Shaha, D. C., & Cho, Y. K. (2016). Salt plug formation caused by decreased river discharge in a multi-channel estuary. *Scientific Reports*, *6*, 27176. https://doi.org/10.1038/srep27176
Sindhu, B., & Unnikrishnan, A. S. (2013). Characteristics of tides in the Bay of Bengal. *Marine Geodesy*, *36*, 377–407. https://doi.org/10.1080/1490419.2013.781088
Speer, P. E., & Aubrey, D. G. (1985). A study of non-linear tidal propagation in shallow inlet/estuarine systems. Part II: Theory. *Estuarine, Coastal and Shelf Science*, *21*, 207–224. https://doi.org/10.1016/0272-7714(85)90097-6
Syvitski, J. P. M., Kettner, A. J., Overeem, I., Hutton, E. W. H., Hannon, M. T., Brakenridge, G. R., et al. (2009). Sinking deltas due to human activities. *Nature Geoscience*, *2*, 681–686. https://doi.org/10.1038/NGEO629
Syvitski, J. P. M., & Saito, Y. (2007). Morphodynamics of deltas under the influence of humans. *Global and Planetary Change*, *57*, 261–282. https://doi.org/10.1016/j.gloplacha.2006.12.001
Tejedor, A., Longjas, A., Zaliapin, I., & Foufoula-Georgiou, E. (2015). Delta channel networks: 2. Metrics of topologic and dynamic complexity for delta comparison, physical inference, and vulnerability assessment. *Water Resources Research*, *51*, 4019–4045. https://doi.org/10.1002/2014WR016604
Todeschini, I., Toffolon, M., & Tubino, M. (2008). Long-term morphological evolution of funnel-shape tide-dominated estuaries. *Journal of Geophysical Research*, *113*, C05005. https://doi.org/10.1029/2007JC004094
Toffolon, M., & Todeschini, I. (2006). Channel competition in tidal flats. In G. Parker, & M. H. García (Eds.), *River, coastal and estuarine morphodynamics: RCEM 2005–Proceedings of the 4th IAHR symposium on river, coastal and estuarine morphodynamics* pp. 653–651). London: CRC Press.
Wells, J. T. (1995). Tide-dominated estuaries and tidal rivers. In G. M. E. Perillo (Ed.), *Geomorphology and Sedimentology of Estuaries* pp. 179–295), chap, 6. Amsterdam: Elsevier.
Wilson, C., & Goodbred, S. L. (2015). Construction and maintenance of the Ganges-Brahmaputra-Meghna delta: Linking process, morphology, and stratigraphy. *Annual Reviews of Marine Science*, *7*, 67–88. https://doi.org/10.1145/annurev-marine-010213-135032
Wilson, C., Goodbred, S., Small, C., Gilligan, J., Sams, S., Mallick, B., & Hale, R. (2017). Widespread infilling of tidal channels and navigable waterways in human-modified tidal deltaplain of southwest Bangladesh. *Elementa*, *5*, 78. https://doi.org/10.1525/elementa.263
Winterwerp, J., & Giardino, A. (2012). Assessment of increasing freshwater input on salinity and sedimentation in the Gorai river system: Report to World Bank (*Tech. rep.*) Delft: Deltares. https://doi.org/10.13140/2.1.1504.1286
Wright, L. D., Coleman, J. M., & Thom, B. G. (1973). Processes of channel development in a high-tide-range environment: Cambridge Gulf-Ord River Delta, western Australia. *The Journal of Geology*, *81*, 15–41. https://doi.org/10.1086/627805
Zeff, M. L. (1988). Sedimentation in a salt marsh-tidal channel system, southern New Jersey. *Marine Geology*, *82*, 33–48. https://doi.org/10.1016/0025-3327(88)90005-9
Zeff, M. L. (1999). Salt marsh tidal channel morphometry: Applications for wetland creation and restoration. *Restoration Ecology*, *7*, 205–211. https://doi.org/10.1046/j.1526-100X.1999.72013.x
Zhang, W., Feng, H., Hoitink, A. J. F., Zhu, Y., Gong, F., & Zheng, J. (2017). Tidal impacts on the subtidal flow division at the main bifurcation in the Yangtze River Delta. *Estuarine, Coastal and Shelf Science*, *196*, 301–314. https://doi.org/10.1016/j.ecss.2017.07.008

References From the Supporting Information

Angamuthu, B., Darby, S. E., & Nicholls, R. J. (2018). Impacts of natural and human drivers on the multi-decadal morphological evolution of tidally-influenced deltas. *Proceedings of the Royal Society A*, *474*, 26. https://doi.org/10.1098/rspa.2018.0396
Friedrichs, C. T., & Aubrey, D. G. (1994). Tidal propagation in strongly convergent channels. *Journal of Geophysical Research*, *99*, 3321–3336. https://doi.org/10.1029/93JC03219
Godin, G. (1972). *The analysis of tides*. Toronto: University of Toronto Press.
Guo, L., van der Wegen, M., Roelvink, J. A., & He, Q. (2014). The role of river flow and tidal asymmetry on 1-D estuarine morphodynamics. *Journal of Geophysical Research: Earth Surface*, *119*, 2315–2334. https://doi.org/10.1002/2014JF003110
Jay, D. A., & Flinchem, E. P. (1999). A comparison of methods for analysis of tidal records containing multi-scale non-tidal background energy. *Continental Shelf Research*, *19*, 1695–1732. https://doi.org/10.1016/S0278-4343(99)00036-9
Savenije, H. H. G. (2005). *Salinity and tides in alluvial estuaries*, pp. 194. New York: Elsevier.